IEEE Robotics and Automation Letters (RAL) paper presented at
2024 IEEE/RSJ International Conference on Intelligent Robots and Systems (IROS)
October 14-18, 2024. Abu Dhabi, UAE

A Novel Friction Measuring Method and Its Application to Improve the Static Modeling Accuracy of Cable-Driven Continuum Manipulators

Yicheng Dai, Sheng Wang, Xin Wang, and Han Yuan, *Member, IEEE*

***Abstract*—Cable-driven continuum manipulators exhibit high flexibility and dexterity, leading to their increased popularity in recent years. Friction analysis is a crucial problem for these manipulators. Previous research has introduced friction models that are applicable to dynamic states where the direction of friction can be ascertained. However, in static states, the direction of internal friction remains undetermined. Additionally, previous studies have investigated the friction law within a single cable hole. However, as multiple cable holes exist along the manipulator, friction should be considered as a series of forces and examined across multiple cable holes. Measuring internal friction presents a challenge due to the unique structure of the manipulator. To our knowledge, no state-of-the-art research has studied how to measure the friction along the entire manipulator. In this letter, we propose a novel friction measuring method based on fiber Bragg grating (FBG) sensors. Experimental results show that the friction distribution can be fully measured. We apply this method to a static model and shape estimation experiments demonstrate that the accuracy of the static model is significantly improved, particularly when the friction has inconsistent directions. Our proposed friction measuring method provides a valuable approach for mechanics analysis of cable-driven continuum manipulators.**

***Index Terms*—Cable-driven continuum manipulator, friction measuring, fiber Bragg grating (FBG) sensors.**

I. Introduction

CONTINUUM robots are characterized by their ability to bend and deform along their entire length, emulating the biological structures of snakes, elephant trunks, and octopus tentacles [1], [2]. They have been found applications in various fields, including invasive surgery [3], gas turbine engine maintenance [4] etc. Despite the advantage of low inertia of the manipulator's arm, the special actuation mechanisms, where actuators are located away from the end-effectors, bring inherent uncertainties due to backlash effects, compliance, and friction in the actuation lines [5]. These uncertainties can limit the precision of the manipulators.

Many studies on cable-driven continuum manipulators have assumed that the transmission of force from motor torques to remote links is lossless [6]. For example, a classic model for the statics and dynamics of continuum manipulators was proposed based on the Cosserat-rod and Cosserat-string models [7], but the friction in the interaction between the cables and the channel was neglected. While establishing the analytic formulation for shape restoration of a multi-backbone continuum robot based on elliptic integrals [8], the author assumed that the friction could be ignored. In the workspace analysis of a continuum robot using a static model, the friction was also ignored [9]. Although some research has used lubricating grease to minimize friction between driving cables and disks, this method is not long-lasting as the cable moves back and forth, causing lubrication to disappear and friction to dramatically increase [10]. Low-friction materials can also be used to minimize friction, but frictional forces are expected to increase as the curvature of the manipulator increases due to larger normal forces. Therefore, the neglect of the internal friction between the cables and the disks in these methods will lead to discrepancies and errors between the theoretical results and the experimental results.

In fact, internal friction between cables and disks is the main interference force for tensions [11]. As such, studying friction is crucial for improving the control accuracy and precision of continuum manipulators, which is particularly important for applications such as surgeries where precision is critical. Some researchers have developed friction models to estimate the friction between driving cables and cable holes. For example, an analytical model based on Coulomb friction was developed to describe the influence of frictional effects between the driving cable and its conduit [12]. This model departed from the constant tension assumption used in existing models and predicted the tension distribution along the driving cable. In [13], a velocity-based friction model was used to describe the sliding friction behavior and the direction of friction was determined by the cable length change. In establishing the dynamics of a continuum manipulator, cable-disk friction was analyzed using a continuous saturated viscous friction model, which accurately represented

Manuscript received 4 August 2023; accepted 14 January 2024. Date of publication 7 February 2024; date of current version 26 February 2024. This letter was recommended for publication by Associate Editor S. Caro and Editor C. Gosselin upon evaluation of the reviewers' comments. This work was supported in part by the National Natural Science Foundation of China under Grant 62173114, in part by the Science and Technology Innovation Committee of Shenzhen under Grant JCYJ20210324115812034 and Grant JCYJ20210324115811033, and in part by the Program of Shenzhen Peacock Innovation Team under Grant KQTD20210811090146075. *(Corresponding author: Han Yuan.)*

Yicheng Dai and Han Yuan are with the School of Mechanical Engineering and Automation, Harbin Institute of Technology (Shenzhen), Shenzhen 518055, China, and also with the Guangdong Provincial Key Laboratory of Intelligent Morphing Mechanisms and Adaptive Robots, Key University Laboratory of Space Mechanisms and Robots of Guangdong, Shenzhen 518055, China (e-mail: daiyicheng94@gmai.com; yuanhan@hit.edu.cn).

Sheng Wang and Xin Wang are with the School of Mechanical Engineering and Automation, Harbin Institute of Technology (Shenzhen), Shenzhen 518055, China (e-mail: wangsheng@stu.hit.edu.cn; wangxinsz@hit.edu.cn).

Digital Object Identifier 10.1109/LRA.2024.3363533

dynamic sliding friction when the cable slides [14]. The same method was used to analyze the friction existing in the cable-disk contact area in [15]. However, all these friction analyses are based on the condition that the direction of friction is known to be opposite to the direction of cable sliding. However, when a continuum manipulator changes from a dynamic state to a static state [16], or the manipulator reaches static equilibrium after being disturbed, the static friction in each cable hole is unable to be determined. Moreover, the friction law is usually studied in a single cable hole and then applied to the entire manipulator. In a general cable-driven continuum manipulator, there are multiple disks and cable holes, meaning that friction is a series of forces, each affected by adjacent cable tension and bending angle. Although there are friction models that can evaluate the friction in multiple holes [10], [17], [18], the true value is unknown and the friction models have yet to be verified by experiments. Moreover, in some situations, cable tension may be small. Then the maximum static friction may exceed cable tension and become the dominant force in certain segments. This can lead to an indeterminate and inconsistent direction of friction along the entire cable. However, existing friction models fail to account for situations where friction directions are inconsistent, resulting in a significant discrepancy between real friction and friction model predictions.

The main challenge in characterizing friction accurately is that friction in each cable hole is unknown and difficult to measure [19]. Some researchers have suggested the use of sensors to measure the cable tension. However, these techniques are confined to measuring the tension at either the starting or terminal position of the cable [20], [21]. They remain incapable of obtaining the internal friction within the continuum manipulator. To our knowledge, no existing literature systematically addresses the measurement of friction distribution along the entire driving cable of continuum manipulators. To address this problem, we propose a novel friction measuring method based on FBG sensors, allowing for the determination of friction distribution along the entire manipulator. FBG sensor is a type of sensor that can reflect light of a specific wavelength and it is sensitive to changes in mechanical strain or ambient temperature, which leads to the change of the reflected wavelength [22]. This feature enables the FBG sensors the ability to measure forces, and their force-sensing ability has been verified with high-sensitivity and precision [23]. By using the optical fiber to actuate the continuum manipulator, the FBG sensors can measure the force at the proximal end of the manipulator [20]. A single FBG-based sensor prototype was developed to sense the axial force to help predict the cardiac perforation [24]. The triaxial force-sensing was also studied and accomplished [25]. Other FBG-based methods have also been developed such as estimating the shape or the tip end of continuum manipulators [26], detecting high frequency ultrasound fields [27], or monitoring blood pressure [28]. The wide range of applications of FBGs demonstrates their advantage in measurement.

In this paper, the FBG sensors are used to measure the internal friction in the continuum manipulator. To our knowledge, this is the first study to integrate the optic fiber wire with multiple FBG sensors to measure the friction distribution along the entire driving cable of continuum manipulators. By calibrating the relationship between wavelength changes and forces, FBG sensors can be used as force sensors. While most force sensors measure force at one point only, FBG sensors can provide force measurements of different points using only one probe due to their multiplexing capability. With the dedicated design of the fiber wire, the series of friction along the entire driving cable can be measured by FBG sensors. Taking the optical fiber wire as the driving cable, cable tension in each segment can be obtained, allowing for the obtaining of friction distribution. Furthermore, we apply the friction measuring method to improve the static model and conduct a comparison of shape estimation performance between the methods based on a static model with different friction considerations. Results show that the static model applying the friction measuring method, has the best accuracy. In summary, the proposed friction distribution measuring method addresses a key research challenge for cable-driven continuum manipulators. The main contributions of this paper are as follows:

- A novel method for accurately measuring the friction distribution along the entire cable of cable-driven continuum manipulators is proposed.
- By applying the proposed friction measuring method, we improve the static modeling accuracy.
- Experimental results indicate that the friction exists in each cable hole could be different, particularly when the cable tension is small.

The rest of this paper is as follows. In Section II, the FBG-based friction measuring method is presented. In Section III, a planar continuum manipulator prototype is fabricated and the friction measuring experiment is carried out. In Section IV, the proposed friction measuring method is applied to improve the accuracy of the static model. Shape estimation experiments with different friction conditions were conducted to gauge the accuracy of static models with different friction considerations. Finally, conclusions are made in Section V.

II. FBG-Based Friction Measuring Method

FBGs are intrinsic fiber elements in photosensitive fibers, in which Bragg diffraction can cause one wavelength to be selectively reflected. According to the theory of fiber-coupled modes [29], [30], the reflected wavelength can be written as:

$$\lambda_B = 2n_{eff}\Lambda \tag{1}$$

where Λ is the natural period of the grating, n_{eff} is the effective index of refraction of the guided mode. The strain and temperature are the most direct and main factors that affect Λ and n_{eff}. The change of wavelength can be expressed as:

$$\Delta\lambda_B = \lambda_B \cdot [(1 - P_e) \cdot \varepsilon + (\alpha_\Lambda + \alpha_n) \cdot \Delta T] \tag{2}$$

where P_e is the effective elasticity coefficient of the grating. α_Λ and α_n are the thermal expansion coefficient and thermo-optic coefficient. ΔT is the change of temperature. ε is the strain of FBG. It should be noted that the experiments in this paper are carried out in an environment with a constant temperature. Therefore the change of the wavelength $\Delta\lambda_B$ is only affected

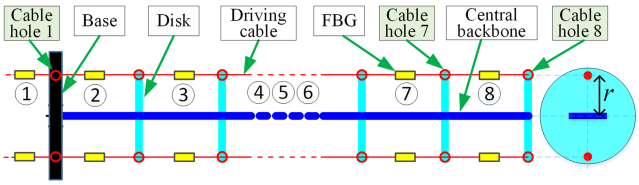

Fig. 1. Illustration of the FBG-based friction distribution measurement.

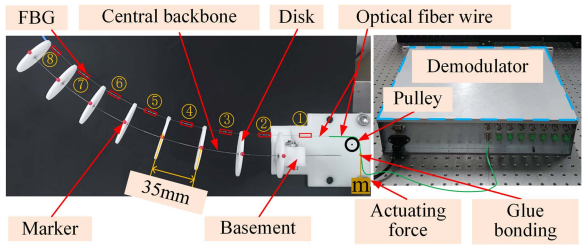

Fig. 2. Experimental setup.

by the strain. Equation 2 can be written as:

$$\Delta\lambda_B = \lambda_B \cdot [(1 - P_e) \cdot \varepsilon] \tag{3}$$

According to (3), the strain shows a linear relationship with respect to the change of wavelength. Furthermore, the strain is related to the mechanical property of the FBG wire. As a result, the force applied to the FBG can be expressed as:

$$T = \frac{\Delta\lambda_B}{\lambda_B \cdot (1 - P_e)} \cdot E_f \cdot A_f \tag{4}$$

where T is the tension at the Bragg grating, E_f is the Young's modulus of the optical fiber, and A_f is the cross-section area of the optical fiber wire. The above equation can be simplified as:

$$T = f(\Delta\lambda_B) \tag{5}$$

To measure friction distribution along the entire manipulator, the fiber wire should be used as the driving cable, with an FBG in each segment of the manipulator to measure the wavelength and cable tension. The layout of the FBGs on a continuum manipulator is shown in Fig. 1. When the manipulator deflects, the FBG will not pass through cable holes and each FBG only moves within its original segment. The largest displacement $D_{\max}$ occurs in the grid near the base. It can be approximately expressed as:

$$D_{\max} = \theta \cdot r \tag{6}$$

where θ is the bending angle of the planar manipulator and r is the radius of the distribution circle of cable holes. In this paper, the maximum bending angle is 114.6°. Through the dedicated design, the wavelength change $\Delta\lambda_B$ corresponds to each segment of fiber wire can be obtained. After knowing the function f in (5) of each FBG, the cable tension of each segment can be known and then the friction distribution can be obtained.

III. Friction Distribution Measuring Experiment

A. Experimental Setup

A planar continuum manipulator prototype is fabricated to illustrate the methodology, as shown in Fig. 2. An optical fiber wire is used as the driving cable (FBGs, Jinan Dahui Photoelectric Technology Shandong, China). The wavelengths of different FBGs are recorded by a demodulator (HG-FBG, Tianjin Huigan Optoelectric Technology Tianjin, China). More demodulation details can be found in [31]. The prototype is actuated by standard weights which are connected to the optical fiber wire. The optical fiber is made using the thermal drawing process, which simultaneously writes the grating and coats the fiber during the fiber draw, ensuring a high strength. Its strength

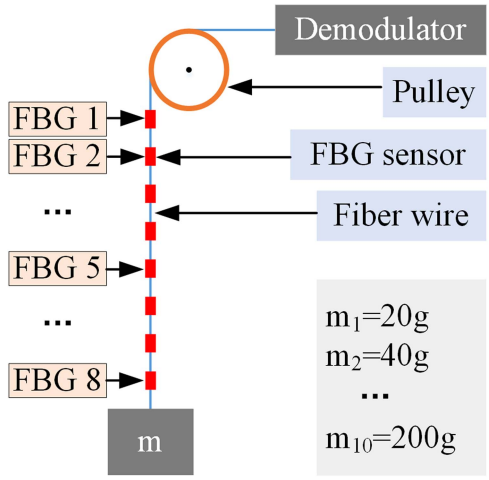

Fig. 3. Calibration process of FBG sensors.

can be further augmented by reinforcing its core [23]. In this paper, the diameter of the cable hole is 0.8 mm. The optical fiber wire is 0.5 mm and the tested load capacity is 4 N. The prototype has 8 disks, each with a thickness of 2 mm. The distance between each two disks is 35 mm, and there is an FBG to measure the tension of the cable. The central backbone is made of steel sheet, with a thickness of 0.3 mm and a width of 6 mm. The diameter of the distribution circle of the cable holes on the disk is 30 mm.

B. The Calibration of FBG Sensors

When measuring the friction distribution using FBG sensors, the relationship between force and wavelength change must first be obtained. For the experimental prototype, there are 8 disks. Hence, the number of the FBG should also be 8. The optical fiber wire is connected to standard weights and the wavelength is recorded. The external load varies from 20 g to 200 g, with an interval of 20 g. The calibration process is shown in Fig. 3 and the results are shown in Fig. 4

Based on (5), the linear fitting function is used to demonstrate the mapping from wavelength to cable tension. It can be written as:

$$T_i = a_i \cdot \Delta\lambda_i + b_i \tag{7}$$

where i represents the i^{th} FBG. a_i and b_i are the parameters of the linear fitting function of the i^{th} FBG. In the fitting process, the least squares method is used to minimize approximation error. After knowing the function of each FBG, forces can be obtained based on the measured wavelength. As shown in Fig. 5,

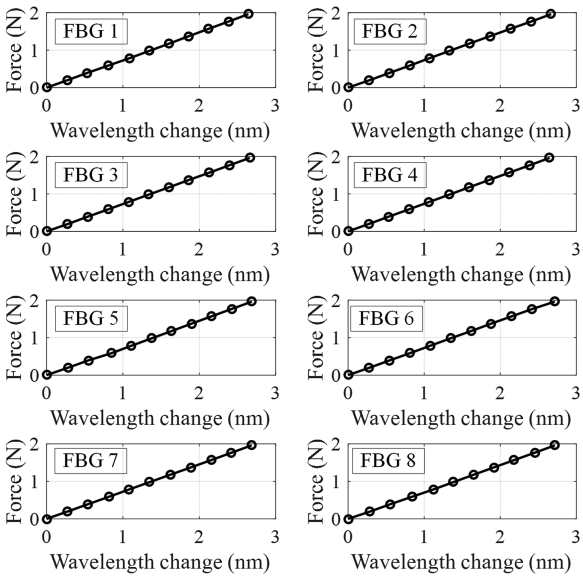

Fig. 4. Calibration of force and wavelength change of FBG sensors.

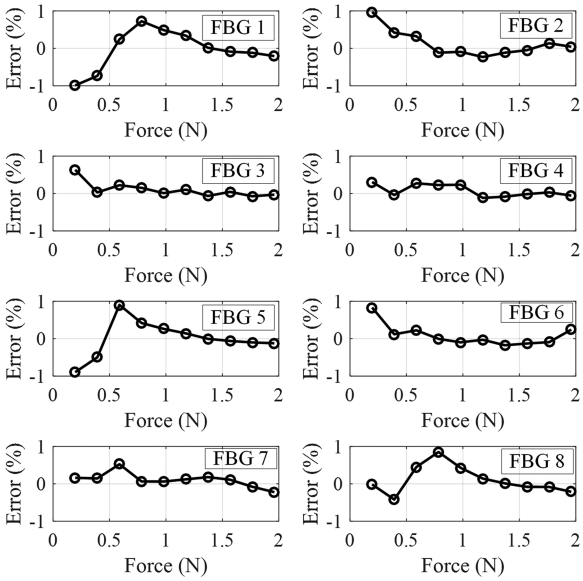

Fig. 5. Force calibration errors of FBG sensors.

the maximum force calibration error of the FBG sensors is no more than 1%, indicating that FBG sensors can be used as force sensors with high precision. This enables the high-precision measurement of internal friction.

C. The Friction Distribution Measurement

In this experiment, the continuum manipulator deflects at different angles, as shown in Fig. 6. The wavelengths of different FBGs are obtained by the demodulator. Based on (7), the cable tension of different segments is obtained. Then the friction in each cable hole is calculated by obtaining the difference between each two adjacent cable tension. The friction values are shown in Fig. 7. As can be seen, the internal friction varies in different cable holes and bending shapes. It is worth noting that there are both negative and positive friction values. This result shows that

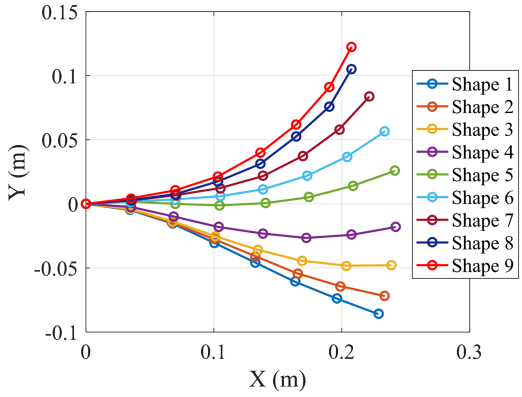

Fig. 6. Different shapes of a continuum manipulator.

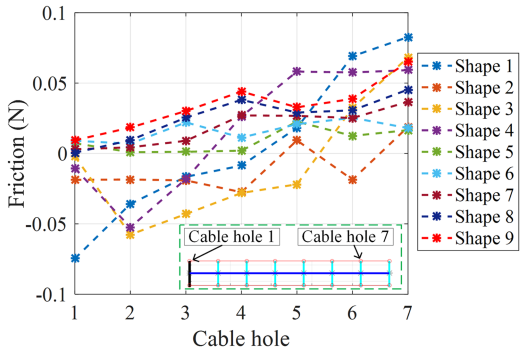

Fig. 7. Friction of different cable holes and shapes.

in some bending shapes (shapes 5, 6, 7, 8, 9), the friction in the manipulator has consistent directions while in other bending shapes (shapes 1, 2, 3, 4), the friction has inconsistent directions.

As we can see in Fig. 6, the bending angles of the first 4 shapes are small, while the bending angles are big for the last 5 shapes. Results indicate that the inconsistency of friction usually occurs when the bending angle of the continuum manipulator is small. When the manipulator is in large deflection, where the resistance force of the central backbone is big, friction in the system has a consistent direction.

IV. Application in Improving the Accuracy of Static Model

For cable-driven continuum manipulators, precise control is closely related to the tension transmission of the cable, and cable-disk friction has a significant impact on this process. Hence, knowing the real friction can improve the accuracy of the static model. In this section, the static modeling process will be recalled and the shape estimation performance will be used to evaluate the model accuracy. Three shape estimation methods are applied, including the static model without considering friction, the static model with friction model, and the static model with friction measuring method. It should be noted that friction models usually work effectively in a dynamic state, where the direction of the friction can be determined. However, in a static state, the direction cannot be determined and the accuracy of the friction model has yet to be verified. Comparisons of the shape estimation performance between these three methods will

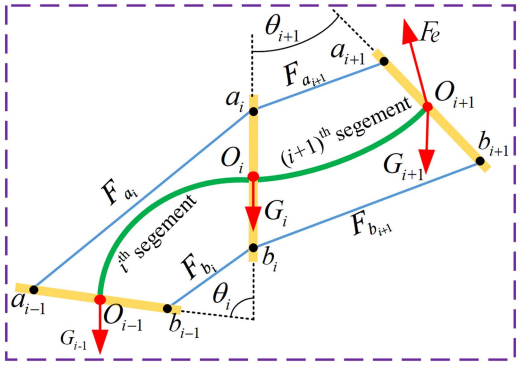

Fig. 8. i^{th} segment of the continuum manipulator.

be conducted in conditions with friction in either the same or different directions.

A. Recall of Static Modeling

In this part, the static modeling process is recalled according to our previous study [10]. In this model, each segment of the manipulator is assumed to be a constant curvature arc and the relative deformation complies with Euler-Bernoulli beam theory. As shown in Fig. 8, the transformation from the $(i-1)^{\text{th}}$ unit R_i can be expressed as ${}^{R_{i-1}}\mathbf{T}_{R_i}$. Then the homogeneous transformation matrix from any local frame R_k $(0 < k \leq m)$ to the base frame R_0 can be written as:

$$ {}^{R_0}\mathbf{T}_{R_k} = \prod_{i=1}^{k} {}^{R_{i-1}}\mathbf{T}_{R_i} \tag{8}$$

Under the effect of cable tension $\mathbf{F}_{a_i}$ and $\mathbf{F}_{b_i}$, the gravity of the spacers and central backbone $\mathbf{G}_{d_i}^{R_{i-1}}$ and $\mathbf{G}_{s_i}^{R_{i-1}}$, and the resultant force $\mathbf{F}_i^{R_{i-1}}$ at point O_{i-1}, the segment reaches equilibrium. The equations can be written as:

$$\mathbf{F}_{i-1}^{R_{i-1}} = \mathbf{F}_{a_i}^{R_{i-1}} + \mathbf{F}_{b_i}^{R_{i-1}} - \mathbf{G}_{d_i}^{R_{i-1}} + \mathbf{G}_{s_i}^{R_{i-1}} + \mathbf{F}_i^{R_{i-1}} \tag{9}$$

$$\mathbf{M}_{i-1} = \mathbf{M}_{a_i} + \mathbf{M}_{b_i} + \mathbf{M}_{d_i} + \mathbf{M}_{s_i} + \mathbf{M}_i + \mathbf{M}_{F_i} \tag{10}$$

where $\mathbf{M}_{a_i}$, $\mathbf{M}_{b_i}$, $\mathbf{M}_{d_i}$, and $\mathbf{M}_{s_i}$ are the moments respectively caused by the cable tensions and the gravity of the spacer and the backbone. $\mathbf{M}_i$ is the resultant moment at point O_{i-1}; $\mathbf{M}_{F_i}$ is the moment by the force $\mathbf{F}_i^{R_{i-1}}$.

It should be noted that, for the first method: static model without considering friction, like previous studies [7], [9], the cable tension is constant, i.e., $F_{a_i}^{R_{i-1}} = F_{a_{i+1}}^{R_{i-1}}$. However, for the second method: the static model with friction model, the coulomb friction model is employed to calculate the friction. Then the cable tension and the friction can be calculated as follows:

$$F_{a_i}^{R_{i-1}} = F_{a_{i+1}}^{R_{i-1}} \pm F_{f_{a_i}}^{R_{i-1}} \tag{11}$$

$$\mathbf{F}_{\mathrm{N}_{a_i}}^{R_{i-1}} = \mathbf{F}_{a_i}^{R_{i-1}} + \mathbf{F}_{a_{i+1}}^{R_{i-1}} \tag{12}$$

$$F_{f_{a_i}}^{R_{i-1}} = \mu \cdot F_{\mathrm{N}_{a_i}}^{R_{i-1}} \tag{13}$$

where μ is the friction coefficient; $F_{N_{a_i}}$ is the normal force generated by the two adjacent cable segments. More details can be found in [10].

For the third method: the static model with measured friction, the real friction value is obtained based on the proposed friction measuring method. Hence, there is no need to calculate the friction, which means (12) and (13) are no longer needed. Equation (11) can be written as:

$$F_{a_i}^{R_{i-1}} = F_{a_{i+1}}^{R_{i-1}} \pm f_{f_{a_i}}^{R_{i-1}} \tag{14}$$

where $f_{f_{a_i}}^{R_{i-1}}$ is a measured value.

The geometric relationship of a segment complies with the Euler-Bernoulli beam theory and the deflection angle θ_i of the i^{th} segment can be expressed as:

$$\theta_i = \frac{M_i \cdot L_i}{E_i \cdot I_i} \tag{15}$$

where L_i is the length of the central backbone; M_i is the bending moment; E_i and I_i are Young's modulus and moment of inertia.

For a continuum manipulator, the static model can be described by these equations and the shape of the manipulator can be estimated.

B. Shape Estimation Experiments

In this part, three methods will be used to estimate the shape of a planar continuum manipulator. The real shape is captured by a camera that detects the marker located at the center position of each disk as shown in Fig. 2. Experimental data of different shapes are represented by the circles. Simultaneously, the outcomes of these three methods are illustrated on the same graph for comparison. Additionally, disk position errors along the arc length are used to gauge the shape estimation performance of the methods against experimental data.

1) The Measurement of Friction Coefficient: When estimating the manipulator's shape using the static model considering friction, the coefficient must first be known. In previous research, the friction coefficient measurement is carried out through a single cable hole. The same experimental procedure is reproduced in this paper. As shown in Fig. 9(a), an identical disk from the continuum robot prototype is vertically fixed. An optical fiber with two calibrated FBG sensors is used as the driving cable. The right end of the optical fiber is fixed and the left end of the cable is attached to a load. The cable tension on both sides of the fixed disk can be measured by the FBG sensors. Note the cable tension on the left side of the disk as F_1 and the tension on the right side as F_2. Note the normal force as F_N, and it can be expressed as:

$$F_N = F_1 \cdot \cos(\theta_1) + F_2 \cdot \cos(\theta_2) \tag{16}$$

Note friction as f and it can be expressed as:

$$f = F_1 - F_2 \tag{17}$$

By changing load, the cable tension changes, as well as the friction and the normal force. As shown in Fig. 9(b), through linear fitting, the friction coefficient can be obtained and the value is 0.1753 in this paper. By taking the value into the friction

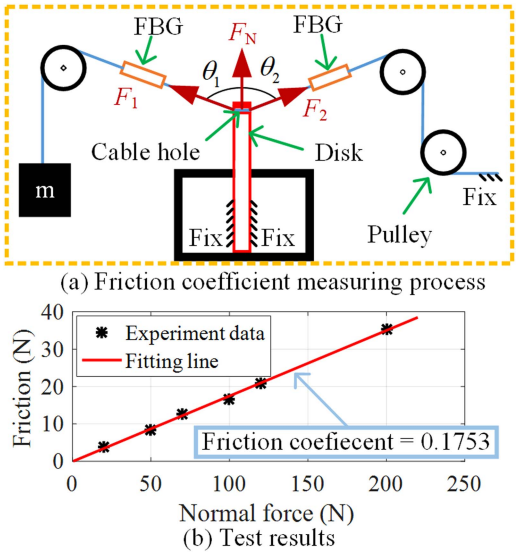

Fig. 9. Friction coefficient measurement in a cable hole.

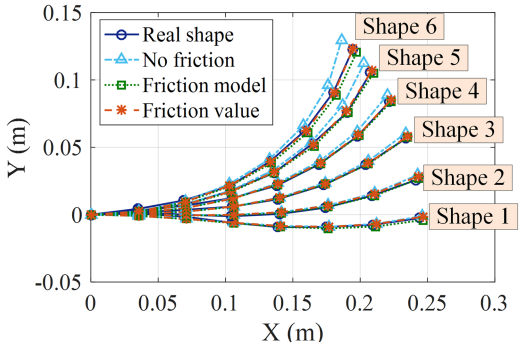

Fig. 10. Shape estimation performance of different methods when the direction of the friction is consistent.

model, the shape of the manipulator can be estimated based on the static model proposed in [10].

2) Experiments With Unidirectional Friction: The deflection of the continuum manipulator is achieved by pulling the driving cables. In the verification of the previous static model [10], there is an assumption that cable tension should never be negative which physically means that the static friction should never take over and play the leading role. To keep cable tension positive, it must be larger than the static friction. Under this condition, 6 groups of tests are conducted and the bending shapes of different methods are shown in Fig. 10.

As shown in Fig. 10, the shapes estimated by the static model without friction are close to the real shapes when the deflection angle is small. However, as the angle increases, the shape estimation performance of this method decreases due to increased friction in the system. The static model using a friction model method shows good performance. The shapes estimated by the static model that applies friction measuring method have a high agreement with the measured shapes. Results show that without considering friction, the static model only works well when the bending angle of the manipulator is small, and its performance worsens with larger bending angles. When friction is considered

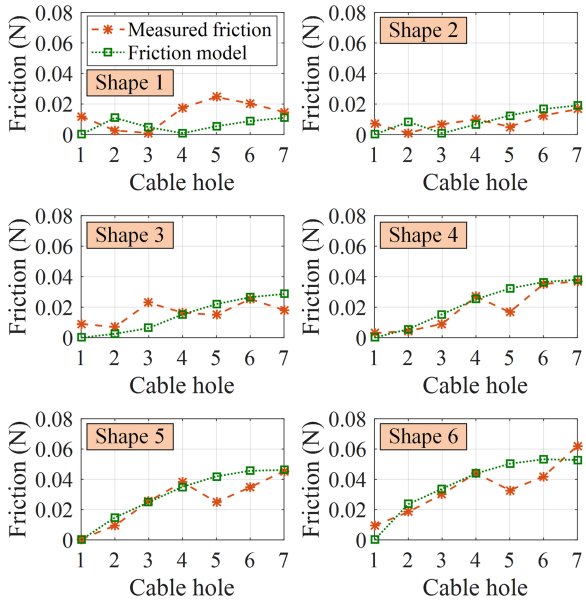

Fig. 11. Real friction and the friction obtained based on static model when the direction of the friction is consistent.

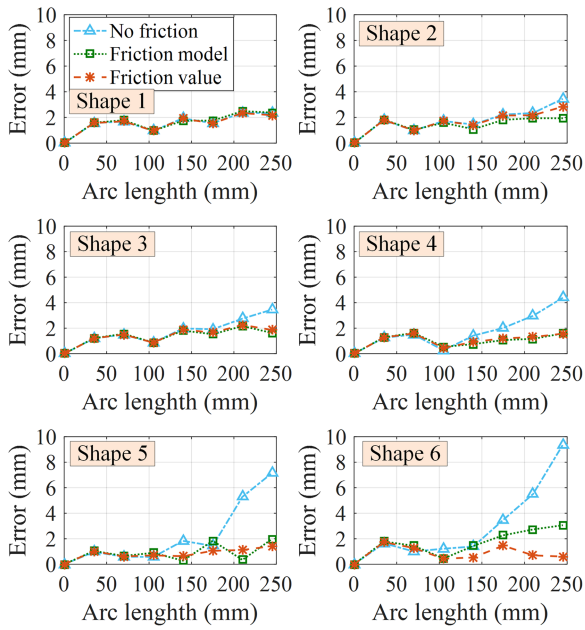

Fig. 12. Shape estimation errors of different methods when the direction of the friction is consistent.

and a friction model is applied, the shape estimation accuracy of the static model is effectively improved.

The friction values for various cable holes and shapes are depicted in Fig. 11. The frictional forces obtained from the friction model closely match the actual friction values measured by the FBG sensors. As a result, the static model, which incorporates either the friction model or the measured friction values, exhibits good shape estimation performance. Fig. 12 shows that under different deflections, the static models without friction and with friction had maximum errors of 9.37 mm and 3.06 mm, respectively. The model with measured friction values had a

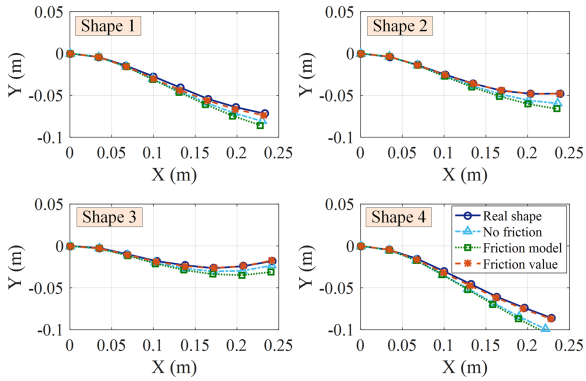

Fig. 13. Shape estimation of different methods when the direction of the friction is inconsistent.

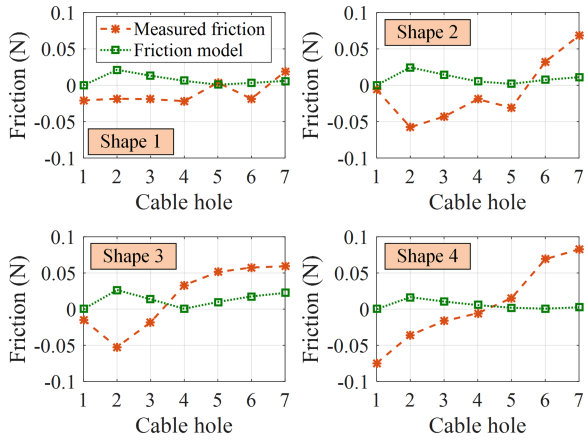

Fig. 14. Real friction and the friction obtained based on friction model when the direction of the friction is inconsistent.

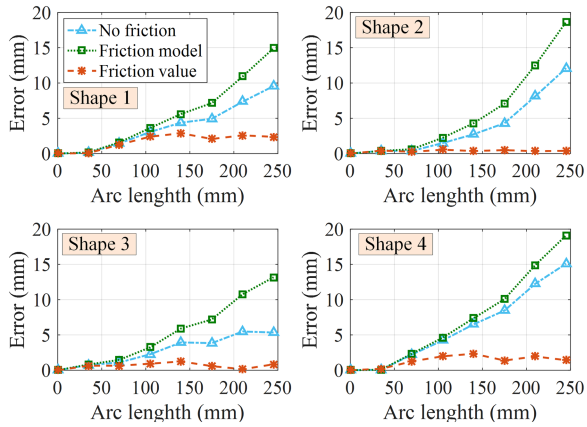

Fig. 15. Shape estimation performance of different methods when the direction of the friction is inconsistent.

lower error of 2.84 mm, improving by 69.69% and 7.19%. The average errors for all six shapes were 5.03 mm and 2.21 mm for the first two models, and 2.03 mm for the third, marking improvements of 59.64% and 8.14%.

It should be noted that the accuracy of the friction model is also high. But it is heavily reliant on unidirectional internal friction. If the direction of friction is inconsistent, which the friction model does not take into account, the accuracy of the static model may be significantly impacted.

3) Experiments With Friction in Different Directions: In some instances, the direction of internal friction in different cable holes may be inconsistent, particularly when cable tension is small. When static friction exceeds cable tension, it becomes the dominant force in certain segments, resulting in an indeterminate and inconsistent direction of friction along the entire cable. The friction model employed in the static model is unable to account for this issue, leading to reduced accuracy. However, if the friction distribution along the entire manipulator can be measured and utilized, the accuracy of the static model can be effectively improved.

Fig. 13 shows that ignoring internal friction in the static model results in large shape estimation errors. Despite incorporating a friction model, the accuracy remains poor. However, using the friction measurement method from Section II to determine actual frictional forces in each cable hole improves the model's shape estimation performance significantly.

Fig. 14 depicts the friction values in different cable holes, with stars representing measured friction and squares representing friction from the model. The measured friction in the four shapes has both negative and positive values, indicating inconsistent frictional force directions. However, the friction obtained from the static model is always positive, suggesting it can't handle friction with inconsistent directions, ultimately resulting in reduced accuracy. The static model with the friction measuring method can fully capture the friction distribution along the cable, eliminating the need for a friction model, and thus accurately estimating the manipulator's shape.

The performance comparison between different methods is shown in Fig. 15. For the four shapes, the static model with no friction and with friction model have maximum errors of 15.1 mm and 19.11 mm, respectively, while the static model with measured friction values has a significantly lower error of 2.87 mm, improving by 80.99% and 84.98%. The average errors were 10.56 mm and 16.47 mm for the first two methods, and 1.75 mm for the third, marking improvements of 83.43% and 89.37%.

These results demonstrate that internal friction in a cable-driven continuum manipulator must be considered. Furthermore, the friction model is unable to account for inconsistent directions of frictional forces along the entire cable, resulting in reduced accuracy for the static model. The friction distribution measuring method proposed in this paper can accurately estimate frictional forces in terms of both direction and magnitude. When this method is applied, the static model exhibits good shape estimation performance.

It is noteworthy that, although the proposed friction measuring method is accurate and effective, it is not feasible for every continuum robot to be equipped with FBG sensors. Therefore, in the future, we will model the friction based on the friction measuring method, so that the friction can be accurately predicted when there is no FBG sensor.

V. Conclusion

In this paper, FBG sensors are utilized to obtain the friction distribution of the entire cable. This research fills a gap in the current literature and provides an accurate approach for

measuring the friction distribution of cable-driven continuum manipulators. Experimental results show that the friction distribution can be fully measured and the direction of friction may differ in different cable holes. Furthermore, we apply this friction measuring method to improve the accuracy of the static model. Shape estimation experiments are conducted to evaluate the accuracy of static models with different friction considerations. Comparison results for different methods demonstrate that, without considering friction, the static model exhibits poor shape estimation performance. When friction is considered and a friction model is employed, the static model exhibits good accuracy under the condition with unidirectional friction, but accuracy decreases when the direction of internal friction is inconsistent. In contrast, by applying the friction distribution measuring method, the static model exhibits good shape estimation performance under conditions with either consistent or inconsistent directions of friction.

The significance of measuring the friction distribution of cable-driven continuum manipulators not only lies in improving the accuracy of the static model, but also lies in mechanics investigation and actuation transmission features to improve the accuracy of this type of manipulator. In fact, this is what we intend to explore in our future research.

REFERENCES

[1] B. Liao et al., "Soft rod-climbing robot inspired by winding locomotion of snake," *Soft Robot.*, vol. 7, no. 4, pp. 500–511, 2020.

[2] E. B. Joyee and Y. Pan, "A fully three-dimensional printed inchworm-inspired soft robot with magnetic actuation," *Soft Robot.*, vol. 6, no. 3, pp. 333–345, 2019.

[3] L. Paterno, G. Tortora, and A. Menciassi, "Hybrid soft–rigid actuators for minimally invasive surgery," *Soft Robot.*, vol. 5, no. 6, pp. 783–799, 2018.

[4] X. Dong et al., "Continuum robots collaborate for safe manipulation of high-temperature flame to enable repairs in challenging environments," *IEEE/ASME Trans. Mechatron.*, vol. 27, no. 5, pp. 4217–4220, Oct. 2022.

[5] R. Roy, L. Wang, and N. Simaan, "Modeling and estimation of friction, extension, and coupling effects in multisegment continuum robots," *IEEE/ASME Trans. Mechatron.*, vol. 22, no. 2, pp. 909–920, Apr. 2017.

[6] Y. Cho, B. Kang, C. Park, and J. Cheong, "Kinematics of elastic tendons for tendon-driven manipulators with transmission friction," *IEEE/ASME Trans. Mechatron.*, vol. 27, no. 1, pp. 202–213, Feb. 2022.

[7] D. C. Rucker and R. J. Webster III, "Statics and dynamics of continuum robots with general tendon routing and external loading," *IEEE Trans. Robot.*, vol. 27, no. 6, pp. 1033–1044, Dec. 2011.

[8] K. Xu and N. Simaan, "Analytic formulation for kinematics, statics, and shape restoration of multibackbone continuum robots via elliptic integrals," *J. Mechanisms Robot.*, vol. 2, no. 1, 2010, Art. no. 011006.

[9] H. Yuan and Z. Li, "Workspace analysis of cable-driven continuum manipulators based on static model," *Robot. Comput.- Integr. Manuf.*, vol. 49, pp. 240–252, 2018.

[10] H. Yuan, L. Zhou, and W. Xu, "A comprehensive static model of cable-driven multi-section continuum robots considering friction effect," *Mechanism Mach. Theory*, vol. 135, pp. 130–149, 2019.

[11] H. Gu, C. Wei, Z. Zhang, and Y. Zhao, "Theoretical and experimental study on active stiffness control of a two-degrees-of-freedom rope-driven parallel mechanism," *J. Mechanisms Robot.*, vol. 13, no. 1, 2021, Art. no. 011018.

[12] G. Subramani and M. R. Zinn, "Tackling friction-an analytical modeling approach to understanding friction in single tendon driven continuum manipulators," in *Proc. IEEE Int. Conf. Robot. Automat.*, 2015, pp. 610–617.

[13] Z. Liu, Z. Cai, H. Peng, X. Zhang, and Z. Wu, "Morphology and tension perception of cable-driven continuum robots," *IEEE/ASME Trans. Mechatron.*, vol. 28, no. 1, pp. 314–325, Feb. 2023.

[14] W. S. Rone and P. Ben-Tzvi, "Continuum robot dynamics utilizing the principle of virtual power," *IEEE Trans. Robot.*, vol. 30, no. 1, pp. 275–287, Feb. 2014.

[15] W. Xu, T. Liu, and Y. Li, "Kinematics, dynamics, and control of a cable-driven hyper-redundant manipulator," *IEEE/ASME Trans. Mechatron.*, vol. 23, no. 4, pp. 1693–1704, Aug. 2018.

[16] Z. Zhao, J. Lu, Q. Wang, C. Liu, and Q. Wang, "The effect of non-spherical aspect of a dimer on the dynamic behaviors," *Nonlinear Dyn.*, vol. 94, pp. 2191–2204, 2018.

[17] A. Gao, Y. Zou, Z. Wang, and H. Liu, "A general friction model of discrete interactions for tendon actuated dexterous manipulators," *J. Mechanisms Robot.*, vol. 9, no. 4, 2017, Art. no. 041019.

[18] P. Rao, Q. Peyron, and J. Burgner-Kahrs, "Shape representation and modeling of tendon-driven continuum robots using euler arc splines," *IEEE Robot. Automat. Lett.*, vol. 7, no. 3, pp. 8114–8121, Jul. 2022.

[19] C. Yang et al., "Geometric constraint-based modeling and analysis of a novel continuum robot with shape memory alloy initiated variable stiffness," *Int. J. Robot. Res.*, vol. 39, no. 14, pp. 1620–1634, 2020.

[20] A. Gao, N. Liu, M. Shen, M. E. Abdelaziz, B. Temelkuran, and G.-Z. Yang, "Laser-profiled continuum robot with integrated tension sensing for simultaneous shape and tip force estimation," *Soft Robot.*, vol. 7, no. 4, pp. 421–443, 2020.

[21] E. Amanov, J. Granna, and J. Burgner-Kahrs, "Toward improving path following motion: Hybrid continuum robot design," in *Proc. IEEE Int. Conf. Robot. Automat.*, 2017, pp. 4666–4672.

[22] K. O. Hill and G. Meltz, "Fiber Bragg grating technology fundamentals and overview," *J. Lightw. Technol.*, vol. 15, no. 8, pp. 1263–1276, Aug. 1997.

[23] R. Karthikeyan, K. Sigmund, Y.-L. Park, and S. C. Ryu, "Performance evaluation of optically sensorized tendons for articulate surgical instruments," *J. Med. Devices*, vol. 13, no. 4, 2019, Art. no. 044504.

[24] S. C. M. Ho, M. Razavi, A. Nazeri, and G. Song, "FBG sensor for contact level monitoring and prediction of perforation in cardiac ablation," *Sensors*, vol. 12, no. 1, pp. 1002–1013, 2012.

[25] A. Gao, Y. Zhou, L. Cao, Z. Wang, and H. Liu, "Fiber Bragg grating-based triaxial force sensor with parallel flexure hinges," *IEEE Trans. Ind. Electron.*, vol. 65, no. 10, pp. 8215–8223, Oct. 2018.

[26] H. Moon et al., "FBG-based polymer-molded shape sensor integrated with minimally invasive surgical robots," in *Proc. IEEE Int. Conf. Robot. Automat.*, 2015, pp. 1770–1775.

[27] N. E. Fisher et al., "Ultrasonic hydrophone based on short in-fiber Bragg gratings," *Appl. Opt.*, vol. 37, no. 34, pp. 8120–8128, 1998.

[28] A. van Brakel, P. L. Swart, A. A. Chtcherbakov, and M. G. Shlyagin, "Blood pressure manometer using a twin Bragg grating Fabry-Perot interferometer," *Proc. SPIE*, vol. 5634, pp. 595–602, 2005.

[29] A. Othonos, K. Kalli, D. Pureur, and A. Mugnier, *Fibre Bragg Gratings*. Berlin, Germany: Springer, 2006.

[30] V. Mishra, N. Singh, U. Tiwari, and P. Kapur, "Fiber grating sensors in medicine: Current and emerging applications," *Sensors Actuators A: Phys.*, vol. 167, no. 2, pp. 279–290, 2011.

[31] C. Huang, W. Jing, K. Liu, Y. Zhang, and G. Peng, "Demodulation of fiber Bragg grating sensor using cross-correlation algorithm," *IEEE Photon. Technol. Lett.*, vol. 19, no. 9, pp. 707–709, May 2007.